# Hydrogeophysical tracking of three-dimensional tracer migration: The concept and application of apparent petrophysical relations

Kamini Singha[1] and Steven M. Gorelick[2]

Received 14 September 2005; revised 21 February 2006; accepted 9 March 2006; published 27 June 2006.

[1] Direct estimation of groundwater solute concentrations from geophysical tomograms has been only moderately successful because (1) reconstructed tomograms are often highly uncertain and subject to inversion artifacts, (2) the range of subsurface conditions represented in data sets is incomplete because of the paucity of colocated well or core data and aquifer heterogeneity, and (3) geophysical methods exhibit spatially variable sensitivity. We show that electrical resistivity tomography (ERT) can be used to estimate groundwater solute concentrations if a relation between concentration and inverted resistivity is used to deal quantitatively with these issues. We use numerical simulation of solute transport and electrical current flow to develop these relations, which we call ''apparent'' petrophysical relations. They provide the connection between concentration, or local resistivity, and inverted resistivity, which is measured at the field scale based on ERT for media containing ionic solute. The apparent petrophysical relations are applied to tomograms of electrical resistivity obtained from field measurements of resistance from cross-well ERT to create maps of tracer concentration. On the basis of synthetic and field cases we demonstrate that tracer mass and concentration estimates obtained using these apparent petrophysical relations are far better than those obtained using direct application of Archie's law applied to three-dimensional tomograms from ERT, which gives severe underestimates.

**Citation:** Singha, K., and S. M. Gorelick (2006), Hydrogeophysical tracking of three-dimensional tracer migration: The concept and application of apparent petrophysical relations, *Water Resour. Res.*, *42*, W06422, doi:10.1029/2005WR004568.

## 1. Introduction

[2] We use cross-well electrical resistivity tomography (ERT) to estimate the distribution of electrical resistivity (the reciprocal of electrical conductivity) in the subsurface. Resistance data are collected by establishing an electrical gradient between two source electrodes and measuring the resultant potential distribution at two or more receiving electrodes. This procedure is repeated for as many combinations of source and receiver electrode positions as desired, and usually involves the acquisition of many hundreds or thousands of multielectrode combinations. Each measured resistance is an average of the electrical properties of both solids and liquids in the system [*Keller and Frischknecht*, 1966]. ERT is sensitive to changes in fluid electrical conductivity and water content [e.g., *Binley et al.*, 2002; *Yeh et al.*, 2002], and has been successfully used to map subsurface transport of conductive tracers [e.g., *Slater et al.*, 2000; *Kemna et al.*, 2002; *Slater et al.*, 2002; *Singha and Gorelick*, 2005].

[3] Geophysical tomographic images often have limited utility for accurately estimating hydrogeologic property values not only because the properties measured in a geophysical survey, e.g., electrical conductivity, dielectric permittivity, or seismic velocity, are often not directly related to the aquifer or groundwater properties of interest, but because the geophysical methods have spatially variable sensitivity and produce inverted results with spatially variable resolution. Empirical petrophysical relations, such as Archie's law [*Archie*, 1942], are often used to connect the geophysical parameter values measured in the field to properties such as water content or tracer concentration. One difficulty with this type of petrophysical translation of geophysical measurements into aquifer or water property values is that the support volume and spatially variable sensitivity of the geophysical measurements are often neglected. Petrophysical relations based on data from a set of wells or cores are most certain near the location where the data were collected. As we move away from the data collection locations into the aquifer, it is more likely that the petrophysical model no longer applies because the underlying processes controlling the physics result in a diminished signal. In particular, geologic heterogeneity, the sensitivity of the geophysical methods, and the effects of image reconstruction enhance the spatial dependence of the petrophysical relation. To overcome these difficulties inherent in the use of geophysical tomography, we develop ''apparent'' petrophysical relations. Apparent petrophysical relations describe the relation between local-scale concentrations and the inverted resistivities from tomographic

[1]Deparment of Geosciences, Pennsylvania State University, University Park, Pennsylvania, USA.
[2]Department of Geological and Environmental Sciences, Stanford University, Stanford, California, USA.


0043-1397/06/2005WR004568

reconstruction. These apparent petrophysical relations are specific to the layout and geometry of data collection, errors, and physics involved. Application of these apparent petrophysical relations to field tomograms allows for better estimates of tracer concentration. *Day-Lewis et al.* [2005] indicate that there is spatially variable resolution with cross-well electrical measurements that must be considered to accurately estimate state variables from tomographic images, and *Yeh et al.* [2002] and *Ramirez et al.* [2005] have looked at stochastic inversion methods to quantify the uncertainty and variability in ERT inversion. Other methods for estimating aquifer properties have recently appeared in the literature; recent work by *Vanderborght et al.* [2005] have used equivalent advection-dispersion equations and stream tube models to quantify breakthrough curves from synthetic 2-D ERT inversions for estimating hydraulic conductivity and local-scale dispersivity values.

[4] Recent work by *Singha and Moysey* [2005] and *Moysey et al.* [2005] has provided a numerical simulation framework for handling the spatial variability in resolution in geophysical surveys and the averaging of heterogeneity from measurements. Simulations based on multiple realizations of hydraulic conductivity are used to expand the small data sets collected in the field into a comprehensive ''database'' that is more representative of the geologic heterogeneity expected in an aquifer. In 2-D synthetic examples, they created multiple realizations of the state variable, either water content or tracer concentrations, and simulated the radar traveltimes or electrical resistances that would be measured in each realization. These ''data'' were then inverted to produce a map of radar velocities or electrical resistivities that correspond to each water content or concentration realization. By considering all realizations at once, they built calibration curves that greatly improve the estimation of state variables from 2-D synthetic tomograms. Although these works are promising, neither considers field data, and the examples were based on realizations of a 2-D synthetic system considering only a single time, or snapshot, and consequently, a temporally invariant relation between dielectric permittivity and water content or electrical resistivity and tracer concentration.

[5] The use of apparent petrophysical relations encompasses a larger issue: quantifying the filter imposed by the geophysical method. To quantitatively use tomographic data, we need to be able to model how geophysical methods sample the subsurface and how parameterization and regularization used in tomographic inversion impacts the estimated image. Recent work by *Day-Lewis et al.* [2005] provide an analytic approach for doing this, however it is limited by the use of a covariance model of spatial variability.

[6] The contribution of this work is an improved approach to estimating state variables for 3-D transient solute transport studies. It involves both synthetic and field data in which solute concentrations are estimated from electrical resistivity tomography (ERT) data. By considering spatially variable apparent petrophysical relations, we build a functional ''geophysical filter'' that converts the inverted geophysical quantity (resistivity) into the fluid property value of interest (concentration). Key to the approach is the apparent petrophysical relation. Each such relation allows us to estimate a local concentration in the aquifer from electrical resistivity given by the tomogram.

[7] The method described here is process based, employing simulation models of solute transport and electrical current through saturated porous media. We provide some examples that delimit when the application of apparent petrophysical relations is most useful, and we demonstrate an approach that is computationally efficient in 3-D: we show that multiple hydraulic conductivity realizations are not always needed for estimation of concentrations with this approach. Rather simulations based on the effective hydraulic conductivity and merely two realizations with different simulated source concentrations are all that is required for specific 3-D scenarios. Our approach using apparent petrophysical relations better estimates tracer concentrations with time lapse ERT than applying Archie's law directly to field tomograms.

## 2. What Is an Apparent Petrophysical Relation?

[8] Electrical resistance data collected in field settings are typically inverted to create tomograms, or maps of electrical resistivity. Values from an inverted resistivity map differ from the ''true'' field resistivities. The ''true'' resistivity is a small-scale value, which we refer to as local resistivity, and is the value of resistivity one would measure if the appropriate volume of rock and water could be removed from the subsurface intact, with appropriate boundary conditions, given the key processes to be studied. The local resistivity in this work is defined as the resistivity at the voxel scale, which is a function of the average solute concentration in that voxel. The local resistivity value differs from that given by inversion of the ERT data collected at the field scale because (1) reconstructed tomograms are often highly uncertain and subject to inversion artifacts, and (2) electrical methods exhibit spatially variable sensitivity; the current density, which defines the sensitivity, diminishes with distance from the source electrode. In addition, the path of the current depends on the electrical resistivity structure of the subsurface as the conductive target migrates with time during a tracer test [*Singha and Gorelick*, 2006]. Consequently, the relation that translates local concentration into inverted resistivity will be spatiotemporally variable. We define the connection between the concentration and the inverted resistivity in each voxel as an apparent petrophysical relation. Any petrophysical relation that does not account for diminished measurement sensitivity with distance from the electrodes and the impact of tomographic reconstruction will not provide accurate estimates of a state variable. Through numerical analogs, we create an extended database of apparent petrophysical relations between concentration and inverted resistivities at each location in space and time.

[9] We suggest the use of an apparent petrophysical relation to quantify the conversion between local concentration and inverted resistivity values at each location. The relation accounts for the effects of regularization (e.g., smoothing) from inversion on the inverted resistivity as well as the ability of ERT to resolve a target. We build the apparent petrophysical relations between local concentration and inverted resistivity through all time and space using simulations of solute transport and electrical flow. By considering multiple realizations, a relation, which is linear in this work, is estimated between the concentration and inverted resistivity at each voxel at each time. These

relations can then be used with field ERT inversions to estimate spatially exhaustive concentration values.

[10] Reconstruction of an electrically conductive target will be better near the electrode locations, and poorer away from the electrodes. Consequently, the relation between concentration and inverted resistivity becomes weaker with increasing distance from the electrodes because the concentrations change greatly compared to the inverted resistivities; as the sensitivity of ERT decreases away from the electrodes, the ability to resolve targets also decreases, and estimated resistivities in the center of the array may be more similar to the background resistivity. Consequently, the slope and intercept of the relation between the concentration and inverted resistivity will change with distance from the electrodes.

[11] Although the empirical relation between electrical resistivity and concentration has been shown to be linear for low salinities [e.g., *Keller and Frischknecht*, 1966], the relation between local concentration and *inverted* resistivity need not be linear. Despite this, we employ a linear apparent petrophysical relation in this work. This choice was based on observed linearity between concentration and inverted resistivities at each location and mathematical simplicity. However, we note that there is nothing explicitly physical about the use of a linear correlation model in this estimation procedure, and other representations, such as probability density functions, may prove to be a better way to describe the relation between concentration and inverted resistivity at any voxel.

[12] The collection of paired concentrations and inverted resistivities on a cell-by-cell basis yields an expanded ''database'' of linear apparent petrophysical relations. Given a resistivity tomogram from inversion of field ERT data, we use that database of apparent petrophysical relations in a predictive manner to estimate the tracer concentration at each location and time. This approach to rock physics can account for the complex physical, geological, and processing effects inherent in electrical tomograms in 3-D field studies. In many field studies, rock physics relations are developed using colocated data at boreholes; unfortunately, those limited data are biased given that ERT sensitivity is best there. By using an expanded database and integrating knowledge of spatial variability in the physics underlying the geophysical method and the effects of regularization, we overcome this issue and produce better estimates of tracer concentrations than those traditionally obtained.

[13] To build the apparent petrophysical relations, two things are required: (1) a notable difference in concentration between a series of two or more realizations and (2) a subsequent difference in inverted resistivities at the same location. If all realizations produced the same concentration value at every voxel, then no relation, linear or otherwise, would exist. The differences in concentration between the realizations can be obtained by varying uncertain system values (e.g., hydraulic parameters, source concentrations), although the goal is to quantify spatially variable resolution, so these realizations can be built in any appropriate manner. Minimally, two realizations are needed to quantify the apparent petrophysical relation at each voxel if a linear relation is assumed.

## 3. Estimation Procedure

[14] The goal of our approach is to estimate concentrations from tomograms of resistivities obtained from inversion of ERT data. To demonstrate the approach, we present the results of two cases, one synthetic and one from field data. In the case of the synthetic model, the entire 3-D map of concentration is known, whereas at the field site, concentration measurements were collected at a centrally located multilevel sampler and a pumping well. As shown in previous work, the best fit relation between the concentration and inverted resistivities from ERT is not the empirical petrophysical relation, but a spatially variable relation [*Singha and Gorelick*, 2006], here taken to be the apparent petrophysical relation. Here, we compare the concentrations derived from electrical resistivity tomograms using the apparent petrophysical relations to those estimated from direct application of Archie's law. The degree to which the two sets of concentrations differ informs us about the geophysical filter that relates the local to the inverted state variable, resistivity.

[15] The central feature of our approach is construction of the apparent petrophysical relation database. A general outline of the estimation procedure is described below, modified from the procedure used for a 2-D synthetic radar case of *Moysey et al.* [2005], and shown in Figure 1.

[16] 1. The first step is flow and transport forward modeling. In the first step, we simulate multiple realizations of the tracer concentration. To create these realizations, we simulate groundwater flow and then advective-dispersive transport, and observe variations in concentration. The choice of the number of realizations used, or how the variability in concentration is produced, will be dependent on the field setting considered. There are few limits on the prior data that can be used to reasonably create variations in concentration. We suggest that known features, such as the field geometry during a field experiment, should be considered known.

[17] 2. The second step is application of an empirical petrophysical model. Each tracer concentration realization is transformed into a local electrical resistivity realization using Archie's law

$$\rho_b = F \cdot \rho_f, \tag{1}$$

where $\rho_b$ is the local bulk electrical resistivity in ohm-m, $\rho_f$ is the fluid electrical resistivity in ohm-m, and $F$ is the unitless formation factor. Resistivity is the inverse of electrical conductivity, which is proportional to solute concentration. Any particular synthetic concentration within a voxel represents the local value, and the use of the experimental petrophysical model (i.e., Archie's law) is justified at the local scale. If the formation factor is unknown, this can be explored parametrically to create multiple series of local resistivity maps from one series of concentration realizations.

[18] 3. The third steps is geophysical forward modeling. A synthetic analog to the ERT experiment conducted in the field is performed on the local resistivity realizations from step 2, thereby creating multiple sets of synthetic resistance measurements. Electrical forward modeling should parallel as closely as possible the actual field experiment in both experimental design and representation of the relevant physical processes.

[19] 4. The fourth step is geophysical inverse modeling. The synthetic resistance measurements obtained via forward

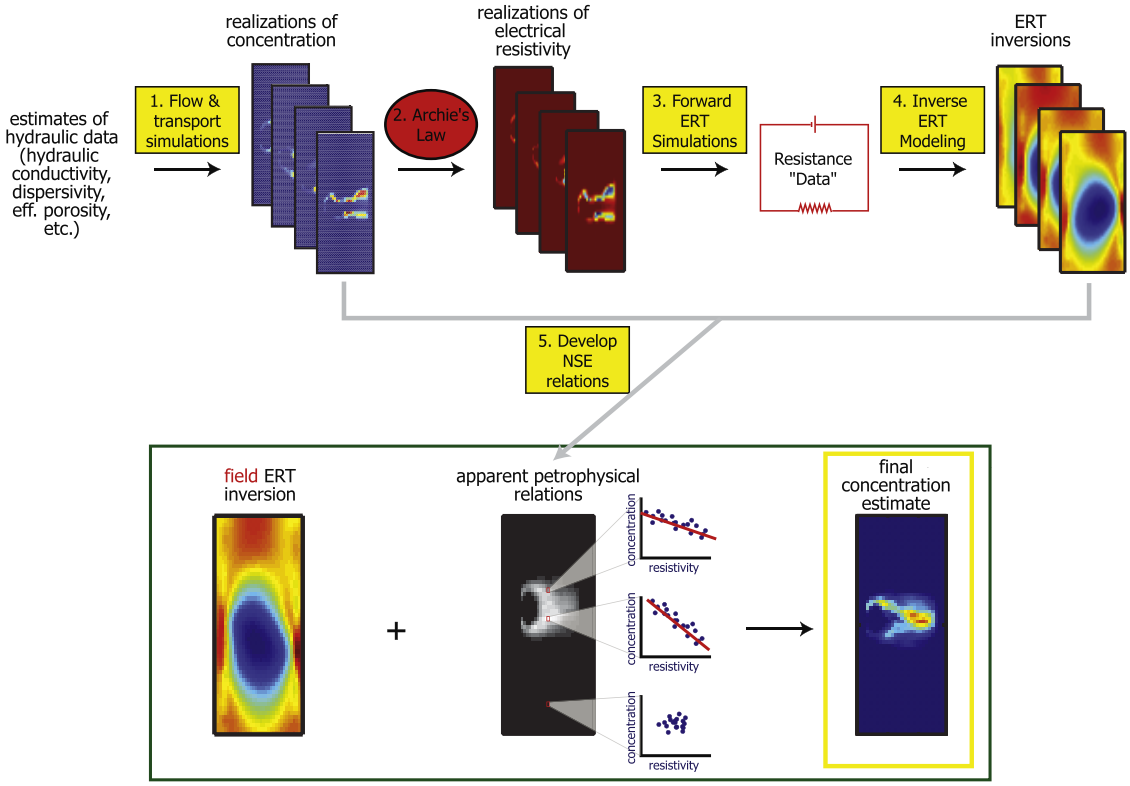


**Figure 1.** Flowchart of nonstationary estimation. Realizations of subsurface concentration are created by flow and transport simulation through multiple hydraulic conductivity maps. The concentration realizations are then converted to electrical resistivity through Archie's law. Following this step, forward and inverse ERT simulation, using the data collection geometry and parameterization used for the field data, is performed. By considering multiple realizations a relation between concentration and inverted resistivity can be built at each voxel, therefore accounting for the spatial variability in the measurement physics and regularization. These relations are applied to a field ERT inversion for a better estimation of concentration than otherwise attainable. Estimation is performed in 3-D but shown in 2-D here.

modeling in the previous step are then inverted for each realization. The inversion of the resistances into resistivity tomograms mimics the inversion of the field ERT data, including the parameterization and selection of regularization criteria. The goal is to closely approximate the processing and inversion steps that have been applied to the field ERT data.

[20] 5. The fifth step is nonstationary estimation. Finally, we use the concentration realizations from step 1 and the subsequent inverted electrical resistivity tomograms from step 4 to calculate the apparent petrophysical relations at every location in space for each snapshot when ERT was conducted in the field. We produce paired sets of concentration and inverted resistivity values at each time and space location: the apparent petrophysical relations. This set of linear relations is then used to convert the resistivities from the ERT tomogram collected in the field to concentrations at any location and time. Throughout the remainder of this paper we will refer to steps 1–5 simply as "nonstationary estimation."

[21] We emphasize that physical processes are incorporated into the procedure using three numerical models and one empirical petrophysical relation: flow and transport models are used to generate the concentration maps, an ERT numerical model of current flow is used to produce forward model resistances, and an empirical petrophysical relation (Archie's law) is used to map concentrations cell-by-cell into local-scale electrical resistivities used in the forward electrical modeling.

## 4. Calculation of Apparent Petrophysical Relations for a Simple Synthetic Example

[22] In this section we present a 3-D synthetic study in which ERT is used to monitor the migration of a saline tracer through the subsurface. For the synthetic case described here, a reference concentration map was simulated using a flow and transport model as described below. We develop the voxel map of apparent petrophysical relations to convert the inverted resistivity tomogram for each snapshot into concentration. The concentrations from this nonstationary estimation process, based on the apparent resistivity relations and Archie's law, were then compared to concentrations estimated using the direct application of Archie's law to the tomograms. We also estimate the tracer mass from the ERT using a modified spatial moment approach, as outlined by *Singha and Gorelick* [2005]. We compare the zeroth moment of the concentrations from nonstationary estimation to that obtained from application of Archie's law to the inverted resistivities as well as the known simulated mass. The goal of the experiment is to accurately reproduce the tracer plume location and concentrations.

### 4.1. Construction of the Reference Concentration Map

[23] The reference concentration map was simulated by considering transport through 3-D hydraulic conductivities generated using SGSIM [*Deutsch and Journel*, 1992]. The random hydraulic conductivities were Gaussian, and the mapped values were based on a spherical variogram with a horizontal range in both the x and y directions of 5.1 m and a vertical range of 0.9 m. Hydraulic conductivity is assumed to be lognormal, with a mean of 115 m/day and a variance of ln(K) of 1. The aquifer thickness is 35 m. Steady state, 3-D, unconfined aquifer flow simulation used MODFLOW-96 [*Harbaugh and McDonald*, 1996], with a voxel discretization of 0.5 m on a side in the area of interest. The boundary conditions on the bottom of the 3-D mesh and two of the vertical faces of the mesh are zero gradient, and an ambient regional hydraulic gradient of 0.001 is set by establishing fixed head boundaries on the other two vertical faces. The effective porosity is 0.35 and the water table is 5.5 m below land surface. An injection and a pumping well are set 10 m apart along the direction of the ambient gradient. An injection rate of 13 L/min and an extraction rate of 39 L/min were used.

[24] After solving for hydraulic heads, transport simulation using MT3DMS [*Zheng and Wang*, 1999] was conducted using the same grid. The transport model simulated the injection of a 2,100 mg/L conservative tracer for 9 hours introduced 14.75–16.25 m below the surface, followed by the injection of water with a background concentration, 60 mg/L. Fixed concentration boundaries equal to 60 mg/L were placed ~100 m from the small subdomain where changes in concentration associated with the tracer test occur. The total extent of the grid covered 270 m in the lateral directions and 160 m in depth. A single time, 6 days after the tracer injection was completed, was considered for the ERT imaging experiment.

[25] After transforming the simulated fluid concentrations in each of the voxels for each snapshot to local resistivity through Archie's law, we simulated the ERT field experiment using a forward electrical flow model using a finite element code (Binley, personal communication, 2006). The resistance data were then inverted to yield the resistivity map imaged by ERT given a stopping criterion based on forward model errors of 2%. The snapshot tomogram is a facsimile of the one that would be obtained from a field application of ERT. The final step is to convert this tomogram into a concentration map. The concentrations are estimated from the inverted resistivity tomogram using two different approaches: (1) Archie's law alone and (2) nonstationary estimation with Archie's law as described below.

### 4.2. Generation of Concentration Realizations and Local Resistivities for Nonstationary Estimation

[26] In this example, the concentration realizations, like the reference concentration map, are obtained using flow and transport simulation. The realizations used for nonstationary estimation are created, in this case, by using the same geostatistical, flow, and transport model parameters as well as boundary conditions as in the previous section. In this case, however, 50 unconditional realizations are developed.

[27] The tracer concentrations were converted to local fluid conductivities (1/resistivity) where 1000 mg/L equals 2000 μS/cm as approximated by *Keller and Frischknecht* [1966]. The fluid conductivity was converted to local bulk conductivity based on Archie's law with a formation factor of 5, and then simply converted to local bulk resistivity. These local bulk resistivities are used in the forward geophysical model.

[28] To demonstrate the nonstationary estimation method for ERT, we selected the concentration distribution on Day 6 after injection for the hypothetical ERT imaging experiment. The choice of day used is not important; in this case we chose a time when the tracer plume was centered between the injection and pumping wells.

### 4.3. Geophysical Forward and Inverse Modeling

[29] Two ERT wells are used for this test. Each is instrumented with 24 electrodes with 1-m electrode spacing. We use a 3-D ERT finite element forward model to detect the tracer plume in 3-D. For the ERT simulations, a nonuniform grid of $50 \times 42 \times 61$ elements was used; our analysis, however, is only focused on the interior of the ERT mesh where the cells are regularly spaced at 0.5 m on a side, which corresponds to the flow and transport mesh in the window area. No-flow boundaries are placed 100 m from the subgrid of interest in each direction. 777 synthetic resistance measurements are collected using an alternating dipole-dipole configuration where each electrode of the current and potential dipoles were in the same well and also split between two wells. The dipole length varied from 1 m to 6 m.

[30] Inverting for the distribution of subsurface resistivity based on measured resistances at ERT wells is a highly nonlinear problem because the current paths through the medium are dependent on the resistivity of the medium. Because of this nonlinearity, this problem is solved using iterative inversion [*Tripp et al.*, 1984; *Daily and Owen*, 1991]. The roughness matrix used in the ERT model regularization is a discretized 3-D second derivative operator. The ERT inversion routine used for this work is based on Occam's approach [*Constable et al.*, 1987; *de Groot-Hedlin and Constable*, 1990; *LaBrecque et al.*, 1996], and the 777 resistance measurements are inverted without noise added in this synthetic example.

### 4.4. Nonstationary Estimation

[31] At each location in the model as defined by each voxel, a unique linear relation between the local concentration and inverted resistivity was fit from the 50 realizations. Each of the 42,200 apparent petrophysical relations was assumed linear and $R^2$ values ranged from 0 in areas outside of the simulated tracer plumes, where no apparent petrophysical relation exists, to 0.66. Each voxel apparent petrophysical relation has a unique slope and intercept that when used with Archie's law, were used to convert the inverted resistivities associated with the reference concentration map to an estimate of concentration in each voxel.

## 5. Results 1: Three-Dimensional Synthetic Estimation

### 5.1. Comparison Between Archie's Law–Estimated and Simulated Concentrations

[32] The reference concentration map is shown in Figure 2a. Comparing this map to the estimate of concen-

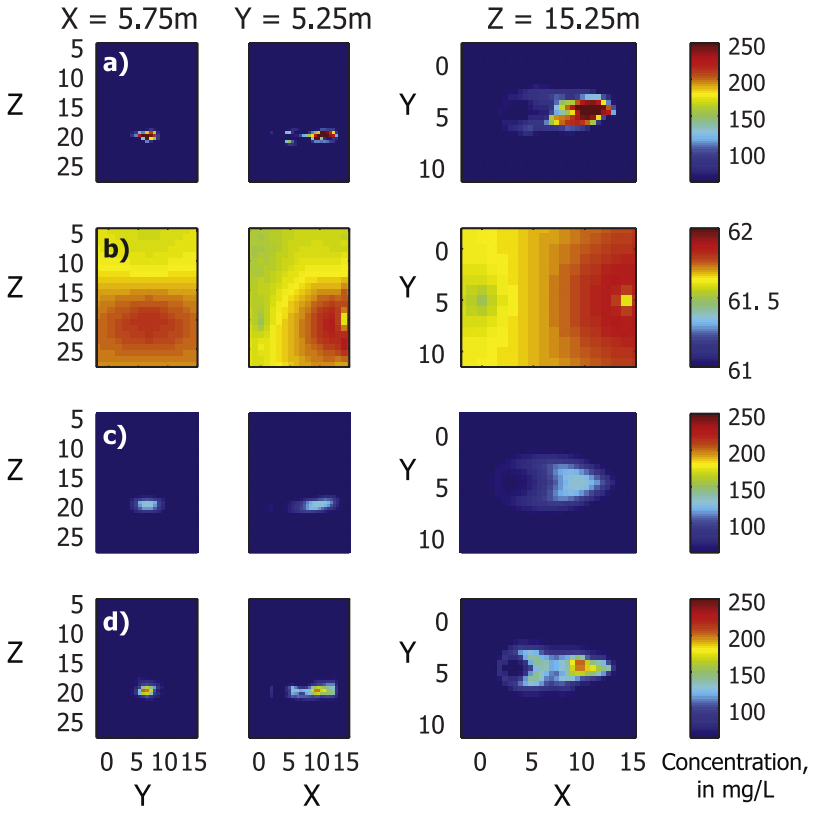


**Figure 2.** Selected slices of 3-D (a) local concentrations as well as concentrations estimated from (b) the synthetic ERT using Archie's law, (c) the mean of the concentration realizations, and (d) the concentration magnitudes from nonstationary estimation for day 6 after tracer injection. All distances are in meters. The concentrations estimated from direct application of Archie's law to the tomograms are much lower than the true concentration, the mean of the realizations, and the results from nonstationary estimation and are consequently on a different color scale.

trations we get from the simple application of Archie's law to the ERT tomogram (Figure 2b) we find that direct application of Archie's law is poor. Inspecting only the "plume area" as defined by the zone within 95% of the simulated concentration peak in excess of the background, we find that the spatial average of the Archie-estimated concentration is only 23% of the actual value. We also note that the variance in concentrations from application of Archie's law directly to the tomogram from the reference map is significantly less than that of the simulated concentrations. The variance of the Archie-estimated concentrations is less than 0.1% of the variance of the true concentration values. Additionally, the mass of the tracer is severely underestimated.

[33] The ERT tomogram, and consequently the concentration estimate, is plagued by troubles common to over-parameterized inverse problems: poor sensitivity of local resistivities to resistance data at the ERT wells coupled with smoothing from regularization used in the inversion algorithm. Without accounting for these difficulties, the estimates of concentration are significantly underestimated, and the actual location of the tracer plume is difficult to ascertain. The concentrations estimated directly from Archie's law are low compared to the true concentrations, which follows from the reconstructed tomograms being overly smooth.

### 5.2. Comparison Between the Mean of the Concentration Realizations and Simulated Concentrations

[34] Figure 2c is the mean of the 50 concentration realizations, and is the map we would obtain from nonstationary estimation if the geophysics contained no information. This map obviously does not accurately capture the detail of the tracer plume; both the shape and magnitude of the concentration plume are incorrect. However, the mean of the realizations is still a better representation of the true field than directly applying Archie's law to the tomogram from the reference map.

### 5.3. Comparison Between Nonstationary-Estimated and Simulated Concentrations

[35] The nonstationary concentration estimate (Figure 2d) gives the best match to the simulated plume shape and concentrations. Application of the apparent petrophysical relations results not only in good recovery of the true tracer concentration peaks, but better mean and variance of the concentration estimates than those estimated directly from Archie's law. Figure 3 shows the histogram of concentrations from the nonstationary estimation, which better fits the histogram of simulated concentrations; the variance of the nonstationary estimated concentrations is more similar to the variance in the simulated concentrations. Although the

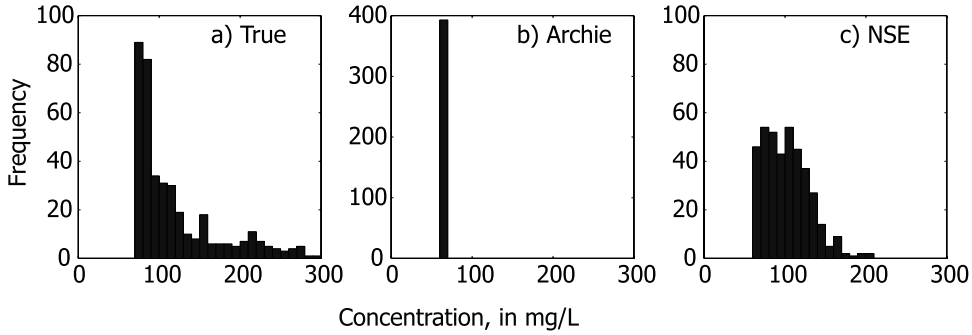


**Figure 3.** Histograms of (a) local concentration and ERT estimated concentration using (b) Archie's law and (c) nonstationary estimation in the 3-D model space for day 6 after injection. The values shown are those that fall within 95% of the concentration peak from the local concentration map.

nonstationary estimation of concentration is not perfect and some underestimation of peak values remains, the values are significantly better recovered than through direct application of Archie's law. A scatterplot (Figure 4) between the simulated and nonstationary estimated concentrations shows that the simulated and estimated concentration values fall more closely to the 1:1 line than those estimated from Archie's law directly, meaning that the magnitude of the concentrations from nonstationary estimation is greatly improved over those estimated from direct application of Archie's law.

[36] The nonstationary estimate of the plume better reproduces the shape of the plume and concentration magnitudes than the estimate obtained by taking the mean of the concentration realizations, indicating that the geophysical data, despite poor resolution away from the electrodes, bring important information to the estimation. By employing apparent petrophysical relations we are able to better estimate the peak concentrations compared to either direct application of Archie's law or the mean of the concentration realizations.

## 6. Description of Field ERT Data Collection and Tracer Test

[37] To test and demonstrate the nonstationary estimation approach for a field experiment, we use the ERT data collected during an unequal strength doublet sodium chloride (NaCl) tracer test in a sand and gravel aquifer, as described by *Singha and Gorelick* [2005]. In their work, ERT was used to track the transport of the NaCl tracer within the region defined by four corner-point wells (Figure 5) at the southern end of the Massachusetts Military Reservation. The mean hydraulic conductivity of the field site is approximately 112 m/d, and the variance in ln(K) is 0.26 [*Hess et al.*, 1992]. Effective porosity has been estimated to be approximately 0.39 [*LeBlanc et al.*, 1991], although a study of the F626 well field described here provided an estimate of 0.28 [*Singha and Gorelick*, 2005]. The field site is downgradient from a sewage treatment facility that discharged secondarily treated effluent from 1936 to 1995 [*LeBlanc et al.*, 1999]. Consequently, the pore fluids onsite are spatially variable, and have total dissolved solids that exceed the concentration in the native groundwater [*LeBlanc et al.*, 1991]. Tracer concentrations were measured 250 times during the 20-day doublet tracer test at a centrally located 15-port multilevel sampler and show preferential injection into the upper part of the aquifer.

[38] Pumping and injection were carried out for an initial 8-day period to achieve a steady state flow regime. First, low electrical conductivity fresh water ($\sigma_f$ = 2.4 mS/m, or 12 mg/L NaCl) was injected into the aquifer for 8 days. Once turned on, the pumping and injection wells continued to run for the duration of the experiment. After 8 days, a 2200 mg/L NaCl tracer ($\sigma_f$ = 470 mS/m) was introduced for 9 hours. A total of 15.3 kg of NaCl were injected into the aquifer. After the 9-hour tracer injection, freshwater injection was resumed for 20 days.

[39] A total of 60 3-D ERT data sets were collected during the tracer test. Each complete 3-D ERT snapshot was collected over 6 hours and consisted of 3150 unique resistance measurements as well as 3150 reciprocal measurements used for error analysis [*Binley et al.*, 1995]. These resistance data were collected using a dipole-dipole configuration that combined current and potential dipoles that were in the same well and also split across two wells. Source pairs were located in all 4 ERT wells at multiple locations in depth. Given an approximate average hydraulic conductivity of 112 m/d, effective porosity of 0.35, and an average estimated pumping/injection hydraulic gradient of 0.0055, the tracer moved approximately 0.4 m during each 6-hour snapshot.

## 7. Calculation of Apparent Petrophysical Relations for Application to the Field Experiment

[40] Using the nonstationary estimation method, we develop apparent petrophysical relations for the tracer test experiment described above. Unlike in the synthetic

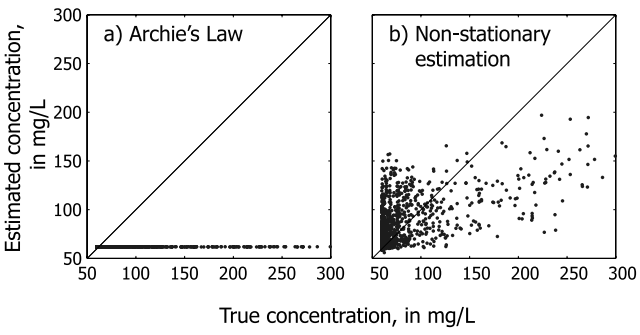


**Figure 4.** Estimated versus local concentrations for the entire 3-D volume after (a) direct application of Archie's law and (b) nonstationary estimation with 1:1 line shown.

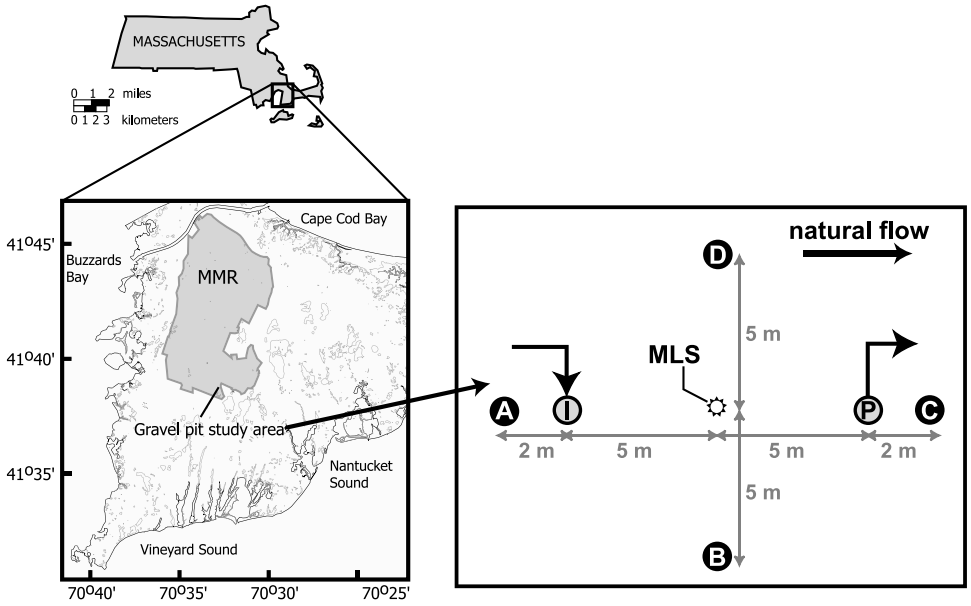


**Figure 5.** Location of field site at the Massachusetts Military Reservation, Cape Cod, Massachusetts, and geometry of experimental well field in map view. ERT wells are labeled A-D. Injection and pumping wells are labeled I and P, respectively. MLS is the multilevel sampler. The distance between ERT wells A and C is 14 m, and the distance between the ERT wells B and D is 10 m.

example, the spatially exhaustive concentration is unknown in the field scenario. Field concentration measurements were collected at the multilevel sampler and pumping well.

[41] To demonstrate the nonstationary estimation method for this case, we selected six snapshots when we have colocated fluid concentration data to compare to the ERT tomograms: Days 4, 5, 6 and 7 after injection, which span the period when the tracer is centered in the array and the center of mass is near the centrally located multilevel sampler; and Days 10 and 12, when the plume peak is near the pumping well. Because the effect of regularization and measurement sensitivity varies through time with the movement of the tracer, each ERT snapshot was considered separately.

[42] The field case is clearly more complicated than the synthetic case presented earlier. Experimental noise will affect the field data quality and the model resolution and, therefore the apparent petrophysical relations. Additionally, the ERT inversions based on resistance data collected in the field do not show the presence of the tracer as clearly as in the synthetic case due to variability of in situ pore fluids.

[43] Two approaches are used to obtain the apparent petrophysical relations. In the first approach, we produce apparent petrophysical relations assuming we don't know the values for important field parameters: hydraulic conductivity, dispersivity, and the Archie formation factor. In the second approach, we demonstrate that multiple realizations based on uncertain parameters are not the only way to produce associations between concentration and inverted resistivity. Instead, we simulate flow and transport based on known estimates of dispersivity, a single effective hydraulic conductivity and two realizations with different simulated source concentrations. This source-scaling method is far simpler than generating numerous random realizations. In our case, it produced reasonable results, and may be extendable to other field scenarios in which source concentrations, for example, are unknown.

### 7.1. Generation of Concentration Realizations and Local Resistivities: Variable Field Parameters

[44] To generate concentration realizations for nonstationary estimation assuming unknown field hydraulic and transport parameters, we simulated tracer migration given a range of plausible homogeneous hydraulic conductivity and dispersivity values. In this case, variability in concentration is a function of uncertain field parameters; however, this need not be the case.

[45] To generate associations between concentration and inverted resistivity, we considered variation in two homogenous hydraulic parameters: the effective hydraulic conductivity (between 90 and 130 m/d), and dispersivity (longitudinal dispersivity between 0.1 and 0.9 m, with the horizontal transverse dispersivity 1/10th of the longitudinal value, and the vertical transverse dispersivity 1/10th of the horizontal), which together control the location and shape of the tracer plume (effective porosity is assumed to be constant and equal to 0.35).

[46] For the model of steady state hydraulic heads, the boundary conditions on the sides perpendicular to flow and the bottom are zero gradient across the boundary, and an ambient, prepumping, hydraulic gradient of 0.001 is set with fixed head boundaries at the inflow and outflow faces of the domain. For the transport model, a background concentration of 60 mg/L was used as initial conditions, with distant fixed concentration boundaries set at 60 mg/L. The pumping regime and tracer injection concentrations are the same as those used in the field example. For the field data, tracer concentrations were related to local fluid resistivities according to a lab-scale relation between concentration and fluid electrical resistivity based on analyses of water samples [*Singha and Gorelick*, 2005].

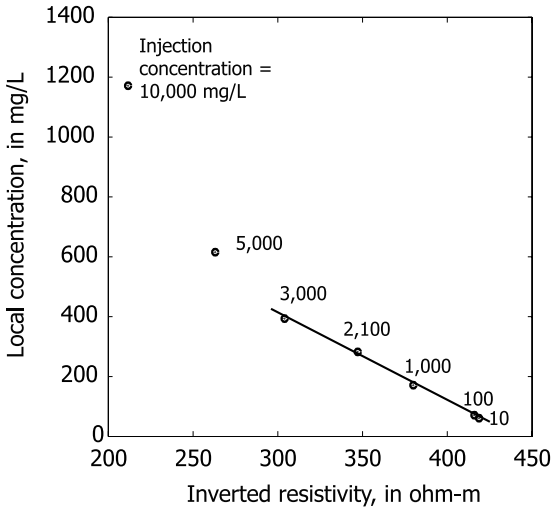


**Figure 6.** Concentration versus inverted resistivity from one voxel of one realization for multiple source injection concentrations. Source injection concentrations are labeled. The relation between concentration and inverted resistivity shown is representative of the voxels traversed by the tracer and indicates that for lower concentrations the relation between concentration and inverted resistivity is approximately linear. At high concentrations the relation becomes nonlinear, but these high concentrations are not expected in this tracer test. This relation changes in space and time.

[47] Additionally, we also consider variability in the Archie formation factor. The local fluid resistivity maps were converted to local bulk resistivities by applying Archie's law assuming a range of spatially uniform formation factors from 3 to 7, which are reasonable given the high porosity sands at the field site [*Wyllie*, 1957]. The resulting local bulk resistivities are used in the forward geophysical model. However, considering variability in the Archie formation factor is not possible given apparent petrophysical relations between concentration and inverted resistivity; one concentration realization may be used to produce multiple local resistivity maps, so there may be no variability in concentration to build appropriate relations. Consequently, we instead consider local resistivity. By varying the hydraulic and transport parameters and the formation factor, we produce different local resistivity and therefore inverted resistivities maps, which in turn allow us to fit associations between the local resistivity and inverted resistivity for each voxel, and then apply Archie's law to estimate concentrations.

### 7.2. Generation of Local Resistivities: Source Scaling

[48] To simulate concentration maps for the source-scaling approach, the geometry of the mesh, pumping rates, boundary conditions, and initial conditions are the same as in the previous step. However, rather than varying the hydraulic conductivity, dispersivity, and formation factor, only the injection source concentration was changed in successive simulations. By using two source concentrations and the same hydraulic information, we produce different concentrations between the two realizations, and therefore meet the requirements to create apparent petrophysical relations at each voxel. As shown in Figure 6 for a representative voxel, transport simulations using tracer-source concentrations ranging over 3 orders of magnitude show that even though the slope between the inverted electrical resistivity and concentration is not linear over 4 orders of magnitude, it is close to linear over at least 3 orders.

[49] The hydraulic conductivity is assumed homogeneous and equal to 112 m/d, and the longitudinal dispersivity equal to 0.1 m. In each of the two simulations, at the single injection well the tracer concentrations were 300 mg/L and 3000 mg/L, respectively. These injection concentrations bound the true source injection concentration of 2200 mg/L. Injection was between 7.0 and 22.2 m below land surface for 9 hours, following and followed by the injection of high-resistivity fresh water of 3 and 30 mg/L with respect to the two simulations with the different injected tracer concentrations. That is, a 100:1 ratio of source to high-resistivity fresh water was maintained in both simulations.

[50] For the source-scaling case, tracer concentrations were related to local fluid resistivities given data collected in the field as in the variable field parameter case. The fluid resistivity map was then converted to local bulk resistivity based on Archie's law using an estimated formation factor of 5.

### 7.3. Geophysical Forward and Inverse Modeling: Variable Field Parameters and Source Scaling

[51] The ERT simulations for both methods used a nonuniform 3-D grid of 50 $\times$ 42 $\times$ 61 elements. Within the area of interest, voxels are 0.5 m on a side. The boundaries are no flow, and a termination strip is used to keep the effect of the boundaries away from the area of interest. For each realization, 3150 measurements are collected between the 4 ERT wells using the same geometry as in the field. For the forward and inverse problem, we used a finite element ERT code.

[52] The 3150 resistance measurements are inverted without noise added in the synthetic example. We used the same grid for the forward ERT model and the field inversions. All snapshot tomograms based on the resistivity realizations use an inversion algorithm employing the same data misfit criterion, 2%, based on the forward modeling error of the synthetic ERT resistances with a homogeneous background. It is important that the inversions for both the numerical analogs and the field data converge to similar error levels. If the fidelity to the data differ, the tomograms will exhibit different degrees of spatial variation, and thus the derived apparent petrophysical relations may not be meaningful.

### 7.4. Nonstationary Estimation: Variable Field Parameters

[53] We build relations between local and inverted resistivity for the subgrid of 42,200 voxels (of 128,100 total), where tracer transport occurs. The realizations with different dispersivity could not be considered together to build a single set of apparent petrophysical relations. Disperse targets are often imaged better than concentrated targets, even if the disperse targets have lower electrical conductivity [*Singha and Gorelick*, 2005]. Consequently, high local electrical conductivities of small size may be imaged less well than lower, more disperse conductivity targets, and the relation between local and inverted resistivity is not meaningful between realizations. To create meaningful associations between the local and inverted resistivity, separate associations are built for each varied physical parameter (hydraulic conductivity, dispersivity) given two different

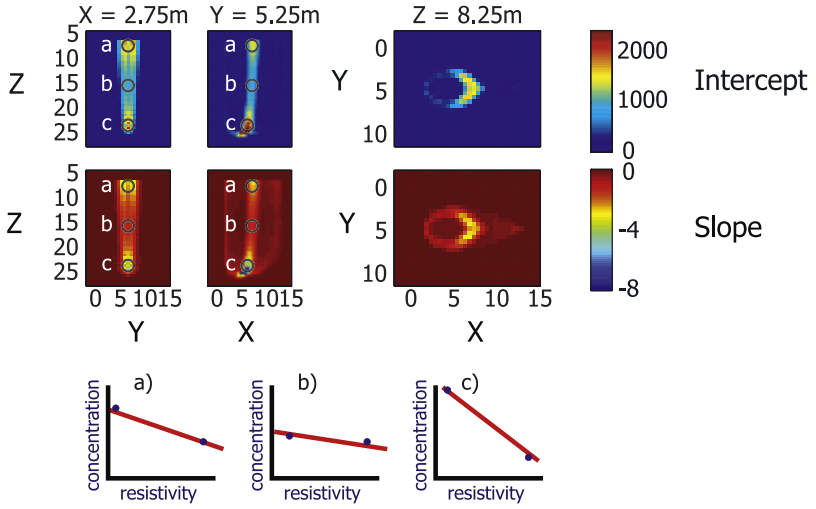


**Figure 7.** Slices through 3-D slope maps from apparent petrophysical relations after application of Archie's law for one time step using the source-scaling method. All distances are in meters. High slope indicates an area where the concentration is high in the given realizations but the inverted resistivity maps are not indicative of its presence. Low slope indicates areas where the relation between the concentration and inverted resistivity is weak. The slopes are related in part to spatiotemporally varying sensitivity.

assumed formation factors. These associations were then used in conjunction with Archie's law generate apparent petrophysical relations, which are then used to produce a series of plausible concentration maps from the field ERT tomograms. Given multiple associations, multiple local resistivity maps and therefore concentration maps are estimated, and we plot these as plausible bounds rather than merely showing an estimate of the mean, which is not representative of any system. Each voxel therefore has a series of local-inverted resistivity associations, each with a unique slope and intercept, that was used to convert the inverted resistivity to estimates of local resistivities in that voxel. Estimates of local resistivity are then converted to concentrations through Archie's law.

### 7.5. Nonstationary Estimation: Source Scaling

[54] For the source-scaling approach, apparent petrophysical relations are built at every voxel given the two concentration realizations. Inspection of the best fit slope and intercept of the relations is instructive (Figure 7). As described earlier, in areas of poor ERT sensitivity, the slopes approach zero, indicating that the inverted resistivities in those locations are nearly the same for all realizations, regardless of the local concentrations. Consequently, the ERT inversions are not capturing the concentration information in the areas of large slopes as well as in other parts of the tomogram. These slopes and intercepts, which make up the apparent petrophysical relations between local concentration and inverted resistivity, are then applied to the field ERT tomograms to estimate spatially exhaustive concentration.

## 8. Results 2: Field Application

[55] For the field data, we use the apparent petrophysical relations (or the association between local and inverted resistivity used with Archie's law) to convert the field tomogram for each snapshot into estimated concentrations. We compare the concentrations from nonstationary estimation to concentrations estimated from direct application of Archie's law to the tomograms for the six time steps: 4, 5, 6, 7, 10, and 12 days after injection. We then calculated the tracer mass in each case.

[56] To better detect the tracer in the geophysical images, we remove the effects of background resistivity associated with spatially variable fluid resistivity by differencing the postinjection from preinjection tomograms. Although it is often preferred to difference the data prior to inversion rather than differencing the tomograms postinversion [*Daily and Owen*, 1991; *LaBrecque and Yang*, 2000], we saw only minor differences between the results of the two methods for the examples considered here.

### 8.1. Comparison Between Archie's Law–Estimated and Field Site Concentrations: Variable Field Parameters and Source Scaling

[57] Figure 8 shows concentration profiles at the multilevel sampler at the six snap shots. The range of concentrations collected at the multilevel sampler over the 6-hour window during ERT data collection is shown in grey. Concentrations based on the simple conversion of ERT tomograms using direct application of Archie's law considering a range of plausible formation factors compare poorly to those measured at the multilevel sampler during the tracer test. As in the synthetic case, the concentrations estimated directly from the ERT inversion using Archie's law are low compared to the measured concentrations. The peak concentration estimated from the ERT is often an order of magnitude less than that measured in the field at the multilevel sampler. However, the concentration measurements at the multilevel sampler indicate that most of the changes in concentration are occurring in the top 20 m of the aquifer, consistent with the results of the field ERT inversions; although the tracer is visible in the differenced inversions down to 15 m, the largest changes occur above 10 m (Figure 9). Although the center of mass from the Archie-estimated concentrations appears to be reasonable,

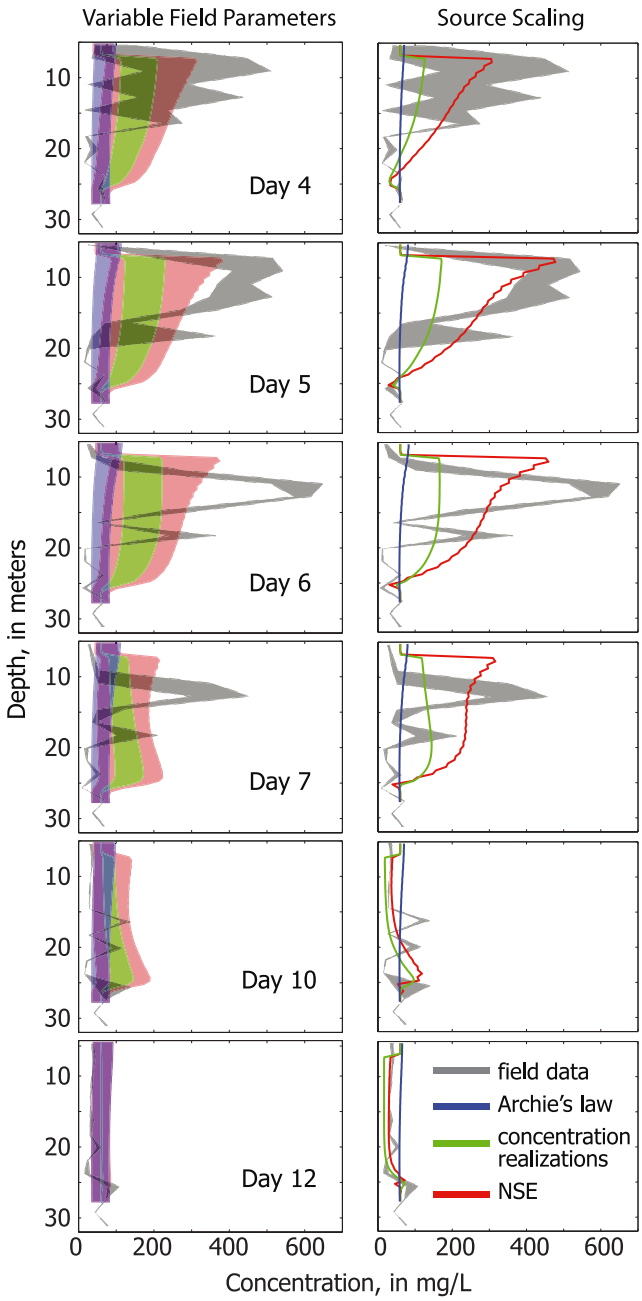


**Figure 8.** Concentration profiles from multilevel sampler location. (left) Values estimated given variable field parameters (and shown as ranges); (right) values using the source-scaling method. Measured field data are shown in gray, with the minimum and maximum values measured over the 6-hour ERT data collection shown in the range. The blue values are the Archie-estimated concentration from the voxels surrounding the multilevel sampler location in the inverted field ERT tomogram. The red values are the concentration profile from nonstationary estimation, which in all cases, provides a better estimate of the multilevel concentration profile measured in the field. Green is the mean of the concentration realizations used to build the apparent petrophysical relations; similarity between the red and green lines indicates little improvement with nonstationary estimation with respect to the assumed hydrogeologic information.

the values are not; this is a function of the inability of ERT to see targets far from the electrodes combined with overparameterization of the inverse problem and the spatially variable effect of regularization. The mass estimated from directly applying Archie's law to tomograms is also too low (Figure 10).

### 8.2. Comparison Between Nonstationary Estimated and Field Site Concentrations: Variable Field Parameters

[58] We compare the concentration maps for each snapshot from nonstationary estimation to field concentration measurements. For the first four times, days 4, 5, 6 and 7 after tracer injection, when the tracer peak is approximately centered over the multilevel sampler, we find that the range of concentration estimates using nonstationary estimation compares more favorably to the field measurements at the multilevel sampler (Figure 8) than either those estimated directly from the tomogram using Archie's law or from the mean of the realizations given the range of plausible formation factors. For these first four times, nonstationary estimation produces qualitatively reasonable concentrations over the 3-D volume in both shape and magnitude given the known injection concentration profile (Figures 9 and 11). The nonstationary estimation shows greater concentration at shallow depth, as seen in the injection profile.

[59] We have limited concentration data at late times (days 10 and 12) to evaluate the improvement of the nonstationary estimation compared to the direct application of Archie's law. Even on days 10 and 12, where very little tracer passes the multilevel sampler, nonstationary estimation concentrations match the measured values at the multilevel sampler. Concentrations were also measured at the pumping well. The measured concentration over the fully screened pumping well at day 10 is 81 mg/L, while the value from nonstationary estimation ranges between 37 and 119 mg/L, depending on the formation factor assumed. The mean value, however, is 78 mg/L, which closely matches the measured concentration. For day 12, we see a similarly wide range: 36 mg/L to 88 mg/L. The mean value, 62 mg/L, is similar to the field-measured concentration of 70 mg/L. Tracer masses estimated using this method have a wide range, as suggested by the wide range in concentrations. Figure 9 shows that the mean over the field site of the nonstationary estimated concentrations is higher and the shape of the plume more reasonable than both the direct application of Archie's law to the tomogram or than the mean of the concentration realizations.

[60] The shape of the estimated solute plume at the multilevel sampler does not perfectly match those measured in the field. This effect is partly an issue of scale; the ERT cannot match the detail measured in the multilevel sampler. Additionally, rate-limited mass transfer provides an explanation for the difference between the nonstationary estimates and the multilevel sampler concentration: ERT is sensitive to both mobile tracer and nonmobile tracer in dead-end pores, whereas the multilevel sampler only measures the mobile tracer. Also, the multilevel sampler concentration data are collected in 1.6 m intervals and every two hours, so it is possible that groundwater with higher concentrations at shallow depths was missed with direct sampling, while still affecting the resultant ERT inversions. We additionally are comparing concentration measurements at one location in x-y space, a mismatch in timing in the simulations used for

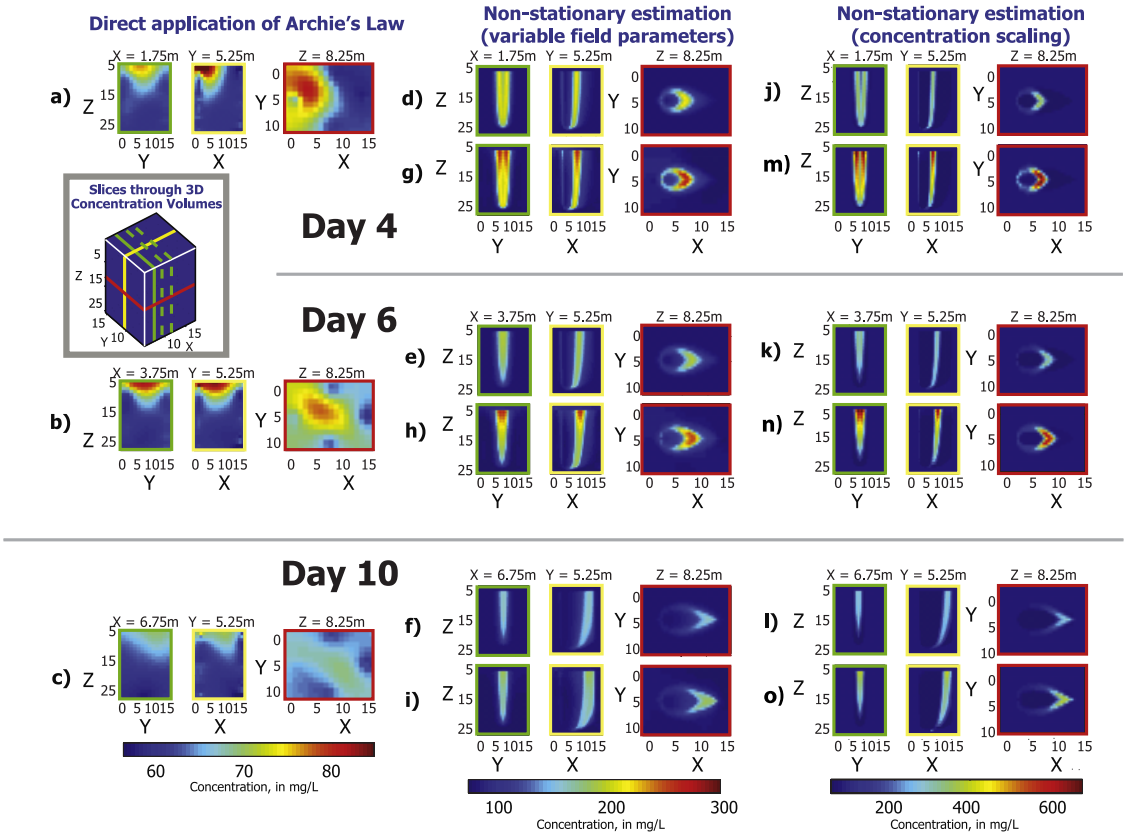


**Figure 9.** Selected slices of 3-D concentrations from three time steps (days 4, 6, and 10 after tracer injection) estimated from (a-c) the field ERT using Archie's law, (d-f) the concentration map estimated from the mean of the realizations used in the nonstationary estimation using variable field parameters, (g-i) the concentration magnitudes from nonstationary estimation using variable field parameters, (j-l) the concentration map estimated from the mean of the realizations used in the nonstationary estimation using concentration scaling, and (m-o) the concentration magnitudes from nonstationary estimation using concentration scaling. Concentration maps in the center are estimated given variable field parameters (the mean value is shown), whereas maps on the right use the source-scaling method. All distances are in meters. Note that the color bar changes between examples so changes in concentration can be seen.

nonstationary estimation by as little as one voxel will change how well the nonstationary estimates match the hard data. A weighted average of neighboring cells may be a more appropriate metric for comparison. Overall, however, nonstationary estimation allows the ERT to do a reasonable job of replicating average tracer concentration profiles measured in the field.

[61] If the concentration realizations used to build the apparent petrophysical relations are not representative of the average behavior of the tracer plume, then there will be limited if any improvement in the results. In cases where entirely incorrect models of the subsurface geology are considered, nonstationary estimation may produce poor results. Despite this, some knowledge of the field conditions in which we work should be known, and uncertainty can be considered through the multiple realization approach described here.

### 8.3. Comparison Between Nonstationary Estimated and Field Concentrations: Source Scaling

[62] Nonstationary estimation based on source scaling also produced a better match to field concentrations than those estimated directly from the tomogram after applying Archie's law. The estimated concentrations generally lie between the maximum and minimum concentration measurements collected at the multilevel sampler over the 6-hour ERT data collection window (Figure 8). The results using source scaling mimic the best case from the unknown field parameter method discussed in the last section. In general, the magnitude and shape of the concentration profiles match well; however, small-scale variability in the multilevel sampler concentrations seen in the field data remain uncaptured.

[63] The measured concentration over the fully screened pumping well at day 10 is 81 mg/L, while the value from nonstationary estimation provides a value of 49 mg/L; clearly this is a poor fit. However, for day 12, both the true and nonstationary values are 70 mg/L. For day 12, the improvement using nonstationary estimation is more significant. The estimated concentrations from the source-scaling method are higher and more focused than those seen from nonstationary estimation using unknown field parameters, as can be seen in Figure 9, but the mismatch in the timing due to fixed estimates for dispersivity, hydraulic conductivity, and effective porosity has a greater impact in the results. Despite this problem, the field inversions show that tracer mass is better predicted when nonstationary estimation is employed

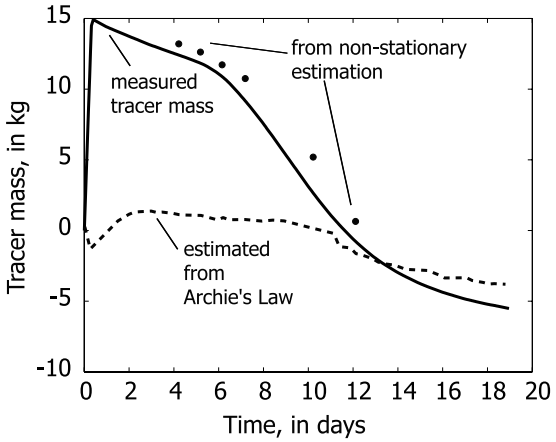


**Figure 10.** True tracer mass in the subsurface calculated from the injected and pumped tracer concentrations and pumping rates compared to tracer mass estimated from (1) Archie's law applied to field ERT tomograms and (2) nonstationary estimation through time. Values are estimated from the source-scaling method. Wide bounds exist for the variable field parameter case, although the mean is similar to the source-scaling method. Nonstationary estimation allows for a better calculation of tracer mass than the traditional application of Archie's law.

(Figure 10), and the nonstationary estimates match the actual tracer mass in the system.

## 9. Discussion and Conclusions

[64] We have presented a method to better estimate tracer concentrations and mass from 3-D field ERT data than traditional methods employing empirical petrophysical models or site specific correlations developed from colocated data. Using process-based models of fluid flow, solute transport, and electrical flow, our nonstationary estimation approach generates apparent petrophysical relations between concentration and inverted resistivity. This nonstationary estimation approach also allows us to integrate our knowledge of local hydrogeology and the effects of spatial variability in the tomogram within an approach that compensates for inversion artifacts and the sensitivity of ERT measurement. Using nonstationary estimation, we are better able to quantify tracer concentrations from ERT, as shown here in both 3-D synthetics and a field example.

[65] Apparent petrophysical relations are built at each voxel location for each snapshot, and provide a means to quantify the spatially variable resolution required for estimation of concentrations based on ERT data. Nonstationary estimation is superior to direct estimation methods that use ERT and the simple application of Archie's law. The approach exploits complementary information about the concentrations contained in imaging provided by geophysical data and underlying hydrogeologic processes reflected in transport modeling results.

[66] Nonstationary estimation is not a cure-all for the difficulties inherent in estimating concentrations based on electrical tomographic inversions. Improvement provided by nonstationary concentration estimation relative to the direct application of Archie's law depends on a number of factors, including (1) the sensitivity of ERT data to the inverted resistivity parameters and (2) the appropriateness of the realizations used in the simulations with respect to the field site hydrogeology. In cases where the geophysical information from ERT is noninformative, nonstationary estimation cannot improve the concentration estimates beyond that given by transport simulation alone. Consequently, when the tracer plume is away from the electrodes and not optimally located for detection using ERT, the geophysical data may hold limited information; although nonstationary estimation will account for spatially variable resolution, it cannot improve the information content of the geophysical data themselves. Additionally, nonstationary estimation will perform no better than information provided to it. Poor estimates of field site hydrogeology, in this case with respect to the average groundwater velocity as dictated by the hydraulic conductivity and effective porosity, may lead to inaccuracies in the location tracer plume and the magnitude

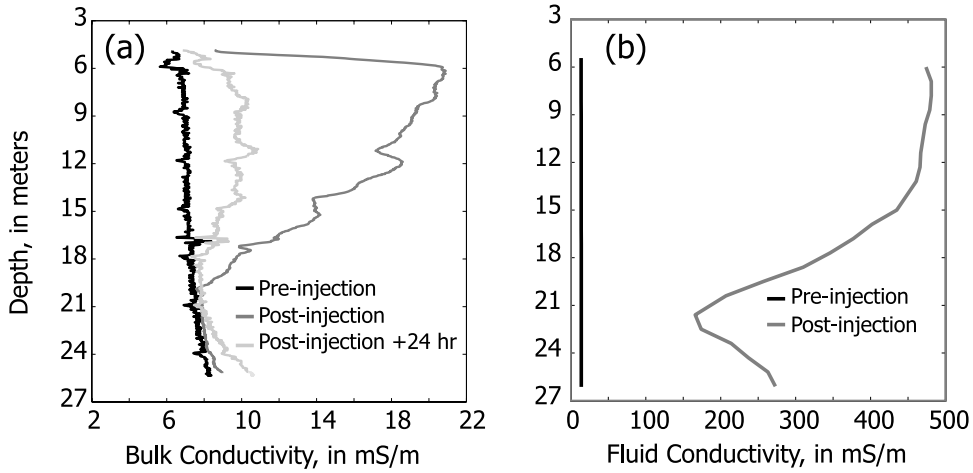


**Figure 11.** Bulk electrical conductivity measured from (a) electromagnetic induction logs and (b) fluid electrical conductivity measured from fluid samples. Data collected prior to tracer injection are shown in black, after the 9-hour injection are shown in dark gray, and 24 hours after injection (electromagnetic induction log only) are shown in light gray. Tracer injection line went to 22.2 m below land surface.

of solute concentrations, and may affect our ability to match data at sampling points, such as those at the multilevel sampler and pumping well shown in our examples.

[67] A strength of the method is its ability to consider variability as shown in the field case where the field parameters are considered unknown. As little or as much variability as desired can be integrated into the framework. However, there is a point where the variability of the realizations used for nonstationary estimation may become so large that the subsequent concentration estimates may be difficult to interpret. The source-scaling method provides an alternative to estimating concentrations from tomograms. This approach provides a means for quantifying the spatially variable ERT resolution with distance from the electrodes using fewer realizations, and a method for estimating concentrations in field scenarios where the source concentration is unknown.

[68] Nonstationary estimation provides a method for (1) going beyond available colocated data at boreholes to develop empirical relations between geophysical estimates; and (2) using hydrologic insight to improve the translation of geophysical results to hydrologic estimates. This is done by constraining our empirical relations to be consistent with (1) a model of spatial variability, (2) hard data at boreholes, and (3) the physics of flow and transport. While we note limitations of this method, the development of simple relations between local and inverted resistivities provides good results of estimated concentration. This approach is a practical alternative to joint inversion of all available data, which would achieve similar results but would be computationally expensive for 4D ERT.

[69] **Acknowledgments.** The authors wish to thank Andrew Binley of Lancaster University for use and instruction on use of his ERT inversion code. The advice and assistance for the field portion of this work of Denis LeBlanc, Kathy Hess, John W. Lane Jr., and Carole Johnson of the U.S. Geological Survey and the support of the USGS Toxic Substances Hydrology Program are gratefully acknowledged. This material is based upon work supported by the National Science Foundation under grant EAR-0124262. Any opinions, findings, and conclusions or recommendations expressed in this material are those of the authors and do not necessarily reflect the views of the National Science Foundation.

## References

Archie, G. E. (1942), The electrical resistivity log as an aid in determining some reservoir characteristics, *Trans. Am. Inst. Min. Metall. Pet. Eng.*, *146*, 54–62.

Binley, A., A. Ramirez, and W. Daily (1995), Regularised image reconstruction of noisy electrical resistance tomography data, paper presented at the 4th Workshop of the European Concerted Action on Process Tomography, Bergen, Norway.

Binley, A., G. Cassiani, R. Middleton, and P. Winship (2002), Vadose zone flow model parameterisation using cross-borehole radar and resistivity imaging, *J. Hydrol.*, *267*, 147–159.

Constable, S. C., R. L. Parker, and C. G. Constable (1987), Occam's inversion: A practical algorithm for generating smooth models from electromagnetic sounding data, *Geophysics*, *52*, 289–300.

Daily, W., and E. Owen (1991), Cross-borehole resistivity tomography, *Geophysics*, *56*, 1228–1235.

Day-Lewis, F. D., K. Singha, and A. M. Binley (2005), Applying petrophysical models to radar traveltime and electrical-resistivity tomograms: Resolution-dependent limitations, *J. Geophys. Res.*, *110*, B08206, doi:10.1029/2004JB003569.

de Groot-Hedlin, C., and S. Constable (1990), Occam's inversion to generate smooth, two-dimensional models from magnetotelluric data, *Geophysics*, *55*, 1613–1624.

Deutsch, C. V., and A. G. Journel (1992), *GSLIB: Geostatistical Software Library and User's Guide*, 369 pp., Oxford Univ. Press, New York.

Harbaugh, A. W., and M. G. McDonald (1996), User's documentation for MODFLOW-96, an update to the U.S. Geological Survey Modular finite-difference ground-water flow model, *U.S. Geol. Surv. Open File Rep., 96-485*, 56 pp.

Hess, K. M., S. H. Wolf, and M. A. Celia (1992), Large-scale natural gradient tracer test in sand and gravel, Cape Cod, Massachusetts: 3. Hydraulic conductivity variability and calculated macrodispersivities, *Water Resour. Res.*, *28*(8), 2011–2027.

Keller, G. V., and F. C. Frischknecht (1966), *Electrical Methods in Geophysical Prospecting*, 523 pp., Elsevier, New York.

Kemna, A., J. Vanderborght, B. Kulessa, and H. Vereecken (2002), Imaging and characterisation of subsurface solute transport using electrical resistivity tomography (ERT) and equivalent transport models, *J. Hydrol.*, *267*, 125–146.

LaBrecque, D. J., and X. Yang (2000), Difference inversion of ERT data: A fast inversion method for 3-D in-situ monitoring, paper presented at Symposium on the Application of Geophysics to Engineering and Environmental Problems (SAGEEP), Environ. and Eng. Geophys. Soc., Arlington, Va.

LaBrecque, D. J., M. Miletto, W. Daily, A. Ramirez, and E. Owen (1996), The effects of noise on Occam's inversion of resistivity tomography data, *Geophysics*, *61*, 538–548.

LeBlanc, D. R., S. P. Garabedian, K. M. Hess, L. W. Gelhar, R. D. Quadri, K. G. Stollenwerk, and W. W. Wood (1991), Large-scale natural gradient tracer test in sand and gravel, Cape Cod, Massachusetts: 1. Experimental design and observed tracer movement, *Water Resour. Res.*, *27*(5), 895–910.

LeBlanc, D. R., K. M. Hess, D. B. Kent, R. L. Smith, L. B. Barber, K. G. Stollenwerk, and K. W. Campo (1999), Natural restoration of a sewage plume in a sand and gravel aquifer, Cape Cod, Massachusetts, *U.S. Geol. Surv. Water Resour. Invest. Rep., 99–4018C*, 245–259.

Moysey, S., K. Singha, and R. Knight (2005), A framework for inferring field-scale rock physics relationships through numerical simulation, *Geophys. Res. Lett.*, *32*, L08304, doi:10.1029/2004GL022152.

Ramirez, A. L., J. J. Nitao, W. G. Hanley, R. Aines, R. E. Glaser, S. K. Sengupta, K. M. Dyer, T. L. Hickling, and W. D. Daily (2005), Stochastic inversion of electrical resistivity changes using a Markov chain Monte Carlo approach, *J. Geophys. Res.*, *110*, B02101, doi:10.1029/2004JB003449.

Singha, K., and S. M. Gorelick (2005), Saline tracer visualized with electrical resistivity tomography: Field scale moment analysis, *Water Resour. Res.*, *41*, W05023, doi:10.1029/2004WR003460.

Singha, K., and S. M. Gorelick (2006), Effects of spatially variable resolution on field-scale estimates of tracer concentration from electrical inversions using Archie's law, *Geophysics*, *71*(3), G83–G91.

Singha, K., and S. Moysey (2005), Accounting for spatially variable resolution in electrical resistivity tomography through field-scale rock physics relations, *Geophysics*, in press.

Slater, L., A. M. Binley, W. Daily, and R. Johnson (2000), Cross-hole electrical imaging of a controlled saline tracer injection, *J. Appl. Geophys.*, *44*(2–3), 85–102.

Slater, L., A. Binley, R. Versteeg, G. Cassiani, R. Birken, and S. Sandberg (2002), A 3D ERT study of solute transport in a large experimental tank, *J. Appl. Geophys.*, *49*, 211–229.

Tripp, A. C., G. W. Hohmann, and C. M. Swift Jr. (1984), Two-dimensional resistivity inversion, *Geophysics*, *49*(10), 1708–1717.

Vanderborght, J., A. Kemna, H. Hardelauf, and H. Vereecken (2005), Potential of electrical resistivity tomography to infer aquifer transport characteristics from tracer studies: A synthetic case study, *Water Resour. Res.*, *41*, W06013, doi:10.1029/2004WR003774.

Wyllie, M. R. J. (1957), *The Fundamentals of Electric Log Interpretation*, 155 pp., Elsevier, New York.

Yeh, T. C. J., S. Liu, R. J. Glass, K. Baker, J. R. Brainard, D. L. Alumbaugh, and D. LaBrecque (2002), A geostatistically based inverse model for electrical resistivity surveys and its applications to vadose zone hydrology, *Water Resour. Res.*, *38*(12), 1278, doi:10.1029/2001WR001204.

Zheng, C., and P. P. Wang (1999), MT3DMS: A modular three-dimensional multispecies model for simulation of advection, dispersion and chemical reactions of contaminants in groundwater systems: Documentation and user's guide, *Contract Rep. SERDP-99–1*, 202 pp., U.S. Army Eng. Res. and Dev. Cent., Vicksburg, Miss.

S. M. Gorelick, Department of Geological and Environmental Sciences, Stanford University, Stanford, CA 94305, USA.

K. Singha, Department of Geosciences, 311 Deike Building, Pennsylvania State University, University Park, PA 16802, USA. (ksingha@psu.edu)